Nuclear Instruments and Methods in Physics Research B 361 (2015) 76–79

Contents lists available at ScienceDirect

Nuclear Instruments and Methods in Physics Research B

journal homepage: www.elsevier.com/locate/nimb

Performance of the rebuilt SUERC single-stage accelerator mass spectrometer

Richard P. Shanks *, Philippa L. Ascough, Andrew Dougans, Paul Gallacher, Pauline Gulliver, Dylan H. Rood, Sheng Xu, Stewart P.H.T. Freeman

Scottish Universities Environmental Research Centre (SUERC), Scottish Enterprise Technology Park, East Kilbride G75 0QF, UK

ARTICLE INFO

Article history:
Received 15 December 2014
Received in revised form 16 July 2015
Accepted 27 July 2015
Available online 19 August 2015

Keywords:
SSAMS
Interference
Accelerator mass spectrometry
^{14}C

ABSTRACT

The SUERC bipolar single-stage accelerator mass spectrometer (SSAMS) has been dismantled and rebuilt to accommodate an additional rotatable pre-accelerator electrostatic spherical analyser (ESA) and a second ion source injector. This is for the attachment of an experimental positive-ion electron cyclotron resonance (ECR) ion source in addition to a Cs-sputter source. The ESA significantly suppresses oxygen interference to radiocarbon detection, and remaining measurement interference is now thought to be from ^{13}C injected as ^{13}CH molecule scattering off the plates of a second original pre-detector ESA.

1. Introduction

The NEC single-stage accelerator mass spectrometer (SSAMS) is a popular model accelerator mass spectrometer for radiocarbon measurement. All such instruments must resolve ^{14}C atoms from abundant interferences. The SSAMS at the Scottish Universities Environmental Research Centre (SUERC) is uniquely bi-polar for experimental analysis of accelerated positive ions and for conventional analysis of negative ions. It is sensible that the measurement interferences are similar in the two polarities, so that results with one polarity might also inform other polarity's application at SUERC, and more generally.

Twin-polarity operation requires two ion sources, a negative-ion sputter source and a plasma source for positive ions, which were originally alternately mounted on a single injector without pre-accelerator electrostatic ion energy analysis. Accordingly straggled reduced-energy ^{16}O from either ion source could be injected along with the ^{14}C, as could ^{13}C as full energy ^{13}CH. Measurements in both polarities suffer from an interference to the ^{14}C particle signal which is centred when the pre-detector electrostatic spherical analyser (ESA) is reduced by ~300 V from the 19.8 kV ESA tune for 290.4 keV ^{14}C. Sputtering synthetic samples with added Al_2O_3 and TiH_2 to increase ^{16}O and ^{13}CH signals has shown correlating interference [1]. The ^{16}O and ^{13}C interferences have also been identified with a temporary additional Wien filter indicating double interferences [2]. A conventionally measured ^{14}C background of 1.5‰M was nevertheless possible by the simple addition of 50 V to the ^{14}C ESA tune setting to reduce the interference contribution to the radiocarbon signal [3]. However, the interference to positive-ion source ^{14}C measurement was still significant [4]. Now we have added a switchable pre-accelerator ESA to both facilitate rapid ion source change for the positive-ion experimentation, and to additionally filter ion energy to address the interferences.

2. Rebuild

To install the new ESA and a second ion source injector it was necessary to dismantle the SSAMS to component parts and to reassemble them elsewhere. The new 45° rotatable-ESA can be used to select from two different ion sources, as shown in Fig. 1. One is the NEC model 134 MC-SNICS Cs sputter ion source that was originally mounted on the SSAMS and is used for routine analysis. The other can be either the SUERC gas-capable 39 MC-SNICS [5] or a Pantechnik S.A. Nanogan 10 GHz electron cyclotron resonance (ECR) ion source used for positive-ion mass spectrometry (PIMS) [6].

The sputter ion sources operate at 45 kV including 6.5 kV cathode potential. The beam from either ion source is injected into the accelerator by a 90° magnet with a fast electrostatic manifold bouncing system (MBS). The MBS is used to select between masses 12, 13 and 14 although typically only 13 and 14 are employed and

* Corresponding author.

http://dx.doi.org/10.1016/j.nimb.2015.07.122
0168-583X/

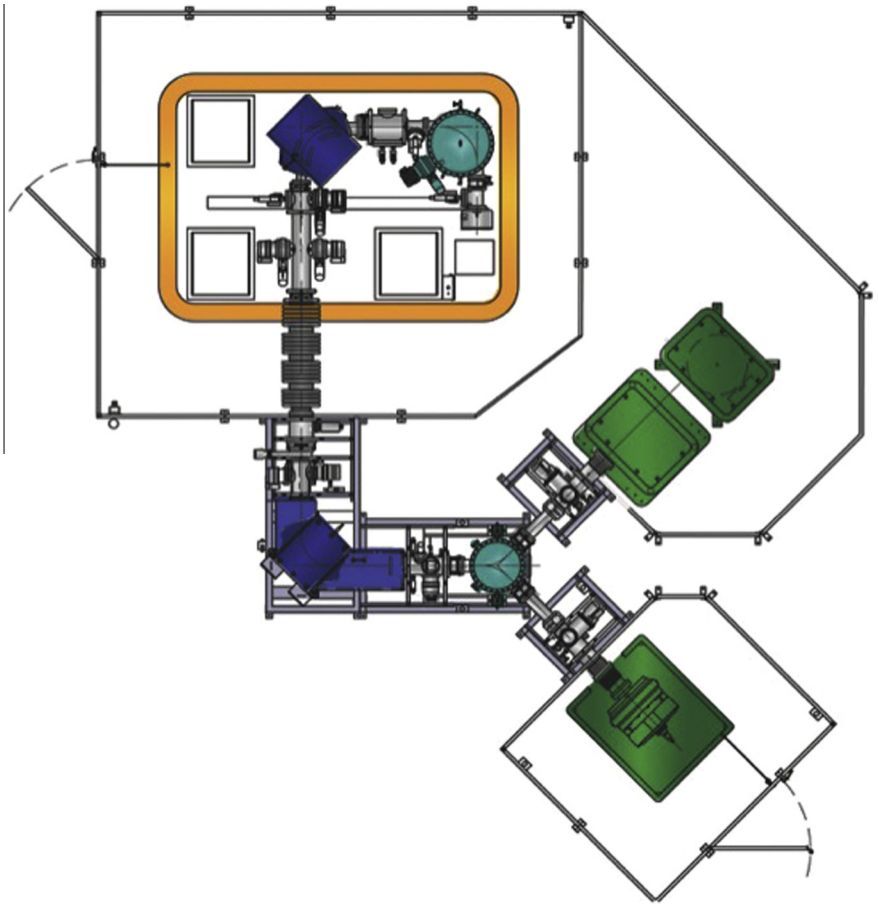

Fig. 1. Schematic of the upgraded SSAMS system. A new rotatable injection-ESA used to select between a 134 MCSNICS Cs sputter ion source and a positive ECR ion source. Also shown as the bipolar 250 kV acceleration platform capable of accepting both positive and negative ions. (Figure provided by NEC).

separately measured $\delta^{13}C$ preferred so that the ion beam size is not constrained by current dependency on the ^{12}C measurement [7]. Next the ion beam is accelerated using the bipolar 250 kV air-insulated deck. In the conventional AMS scheme the C^- ion beam, devoid of short-lived N^- interference, passes through a nitrogen stripper canal where it is converted into C^+ and remaining hydrocarbon interference is largely destroyed in the multiple collisions with the 'thick' stripper gas. A dipole magnet after the stripper selects the $^{12}C^+$, $^{13}C^+$ or $^{14}C^+$. The $^{12}C^+$ and $^{13}C^+$ are measured in off-axis Faraday cups and the $^{14}C^+$ is additionally energy-analysed by a pre-detector ESA before detection with silicon detector. A bounced vertical steer is mounted immediately before the detector to deflect scattered $^{12}C^+$ and $^{13}C^+$ during their injection period and prevent damage to the delicate detector.

To confirm good alignment with minimal losses to the beam, the low-energy to high-energy ion optical transmission of $^{12}C^-$ through the stripper canal without gas was measured over a range of beam currents as shown in Fig. 2. This is uniquely possible with a SSAMS. Up to 97% transmission of the $^{12}C^-$ was measured at low beam currents with good transmission remaining up to 50 μA from both sputter ion sources. ^{13}C and ^{14}C transmission is less current-dependent, and the 14/13 ratio even more so, although this can become unreliable above 150 μA C^-. Accordingly sputtered C^- beams of ~30 μA and ~130 μA are employed depending on whether or not ^{12}C measurement is required.

It is also possible to derive the ^{14}C transmission using standard materials of nominally known carbon isotope ratio. At perfect transmission an OXII sample will produce a detector ^{14}C count rate of ten Hertz per microAmp C^- extracted from the ion source, ignoring fractionation. Accordingly the rebuilt SSAMS routinely achieves 29% ^{14}C transmission through nitrogen stripper to the detector. Prior to the rebuild we would record 32%. The 10% additional beam loss, presumably due to the slightly longer low-energy beam line and the additional beam crossover, is acceptable.

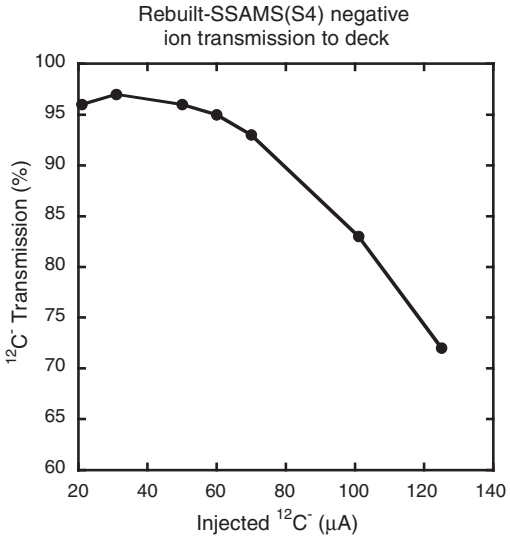

Fig. 2. Ion optical transmission through the accelerator at 250 kV. Low-energy $^{12}C^-$ to high-energy $^{12}C^-$ without stripper gas is a function of $^{12}C^-$ current. High transmission at low beam current indicates good ion optical alignment.

Thousands of samples have now been measured conventionally since the rebuild and without additional external scatter on secondary standards above the reported errors. As expected measurement interference has been somewhat mitigated. A source vacuum-dependent background was previously observed with the SSAMS. After a carousel of samples was loaded into the source the background would remain elevated for the first day. Since the installation of the injection-ESA the source vacuum-dependence no longer exists and a wheel can be installed in the source and measurements started after just a couple of hours of pumping. Also, the pre-detector ESA is operated more close to the ^{14}C-tune. Presumably oxygen is now no longer injected but the ^{13}C remains. Certainly natural-level radiocarbon-PIMS is now possible [6].

3. Remaining interference

An oxygen interference had previously been observed over a large range of the injection magnet field. Sputtered samples with added oxygen were use to create a strong interference signal and a Wien filter was used to identified the oxygen. Oxygen interference, as well as a vacuum related interference, is a problem when trying to measure a sample from CO_2, e.g. with a plasma ion source. The oxygen had a wide range of energies that allowed part of the beam to have the correct magnetic rigidity to be injected into the accelerator. Now the ESA will only transmit a narrow energy range of oxygen beam that would have the wrong magnetic rigidity to be injected into the accelerator. Thus the ESA and the magnet should filter out the oxygen. To test this the scans of the injection magnetic rigidity in [3] were repeated where sputtered background graphite with added Al_2O_3 was measured over a range of MBS values, as shown in Fig. 3. The ^{14}C/^{13}C ratio of an OXII was measured over a range of MBS values shown by the triangle in Fig. 3 before (open symbol) and after (solid triangle) the installation of the injection ESA. The ^{14}C signal is shown to drop away sharply after just a few hundred volts variation in both cases. 300 V was removed from the pre-detector ESA when measuring the interference to maximise the signal (as shown in Fig. 4). The open circles in Fig. 3 show the wide range in magnetic rigidity for ^{16}O prior to the installation of the ESA. After the installation of the ESA the interference of oxygenated background signal (solid circles) is similar to the pure carbon background (diamonds) over the MBS range. This shows that the oxygen interference has been removed. However, the interference from ^{13}C still exists. Samples with added TiH_2, shown by the squares before (open) and after (solid) the installation of the ESA, demonstrates that the ^{13}C interference exists over similar range to the ^{14}C.

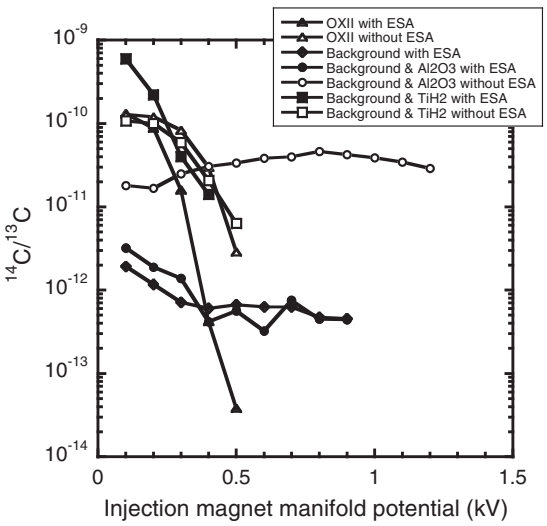

Fig. 3. Scans of the injection magnet manifold chamber bias (normally 100 V) with various sputtered sample materials. The OXII scan was tuned for ^{14}C to demonstrate the acceptance range of the injection magnet. Al_2O_3 and TiH_2 was added to the commercial background graphite to generate interference from ^{16}O and ^{13}CH respectively. The interference scans were measured with the 300 V reduction in the pre-detector ESA to maximise the interference signal shown in Fig. 4.

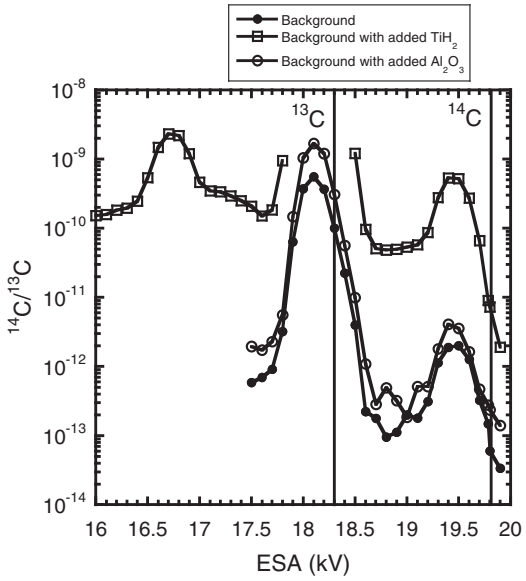

Fig. 4. Scans of the pre-detector ESA with sputtered commercial background graphite and with additional samples adulterated with TiH_2 and Al_2O_3. The optimal settings for the ^{14}C and ^{13}C dissociated from ^{13}CH entering the ESA on axis are indicated.

Scans of the pre-detector ESA are shown in Fig. 4 for sputtered background material (black circles) and with added Al_2O_3 (white circles) and TiH_2 (squares). The operational value for ^{14}C is shown at 19.8 kV. The ESA spectrum has a similar distribution for all of the materials. The ^{14}C is on the shoulder of the first interference peaks, which is centred 300 V below the operational setting. A much larger interference peak is observed 1.5 kV below the operational setting. This signal energy is consistent with ^{13}C dissociated from ^{13}CH. ^{13}C is shown at 18.4 kV with 13/14 the original energy. The interference peak is at a slightly lower energy but this energy shift could be accounted for by a slight loss during the scattering in the high-energy magnet or by the ^{13}C not entering the ESA perfectly on axis. The pure background graphite and the sample with added oxygen have very similar spectra confirming that no additional interference is coming from the oxygen. The sample with the added hydrogen has significantly larger interference peaks with the ^{14}C/^{13}C background rising from 4×10^{-14} to 10^{-11}. The -1.5 kV interference peak, which is attributed to ^{13}C, has significantly increased to the point of saturating the detector. The increase in this peak is to be expected, as the added hydrogen will generate more ^{13}CH for injection. The addition of hydrogen has also increased the -300 V interference peak, which means it must be related to molecular interference. If the ESA scan is continued to lower energies, a third peak is found at -3 kV. The -3 kV and the -300 peaks are of similar intensity and are symmetrically ±1.35 kV either side of the main interference peak.

4. Discussion

^{13}C is injected into the accelerator as a ^{13}CH molecule. When the molecule is broken up in the stripper it should have the wrong mass and energy to be transmitted around the high-energy

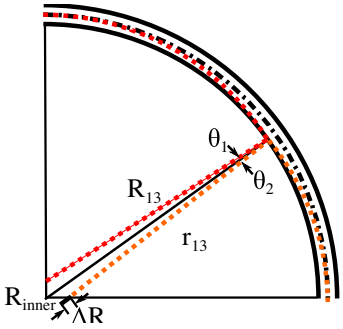

Fig. 5. Accelerator deck ESA schematic showing the trajectory of possible ^{13}C inference. The ^{13}C has a reduced radius of curvature, R_{13}, such that it intersects with the inner radius ESA plate, R_{inner}. A reflected beam with a curvature r_{13}, reduced from R_{13} by ΔR due to energy loss in the refection process will be transmitted from the ESA on axis.

magnet. Some of the stripper gas leaks into the high-energy magnet because the stripper pressure must be run relatively high to destroy the molecules at such low energy. This residual gas in the magnet could result in some scattering of the ^{13}C, a fraction of which leaves the magnet on axis. The ^{13}C only has 13/14 of the energy of the ^{14}C and should easily be removed by the pre-detector ESA.

Fig. 5 shows a schematic of the ESA, the ESA plates are represented by the solid black curves and the trajectory of the ^{13}C around the ESA with the 18.1 kV tune shown by the black chain line. At this setting the ^{13}C is transmitted at 90° to its input trajectory and passes directly to the detector to create the large peak observed in Fig. 4. The ^{13}C radius of curvature decreases so that the carbon moves away from the detector as the ESA potential is increased towards the ^{14}C settings. As the radius continues to decrease the ^{13}C clips or even strikes completely the ESA plate where some of the beam is reflected. If the ion beam is reflected with the same average angle as it impinges on the plain of the ESA plate, such that $\theta_1 = \theta_2$, and the reflected beam has the same ion energy, then the collision point would need to be at the mid-point of the plate for the ion beam to exit the ESA on axis, i.e. the beam would need to reflect symmetrically around the collision point. However the ^{13}C trajectory curves with a radius R_{13}, shown by the red curved line in Fig. 5, and intersects with the inner plate of the ESA, with radius R_{inner}, approximately 2/3 of the way around the plate, at the value of the observed interference peak (19.45 kV). A reflected ion beam with the same energy does not curve enough to exit on axis and misses the detector. The ion beam will however, lose energy during the reflection process such that it has a reduce radius of curvature, denoted by r_{13} and represented by the orange curved line in Fig. 5. The reduction in the radius, $\Delta R = R_{13} - r_{13}$, is also the loss in energy of the ion beam. The loss needs to be 2% for the ion beam to exit on axis at a 19.45 kV ESA setting. (A similar process occurs as the ESA setting is decreased to 16.75 kV and ^{13}C is reflected by the outer plate.) The reflected beam might be expected to have a large scattering angle due to surface imperfections on the plate, etc., however the narrow width of the 19.45 kV interference peak in Fig. 4 suggests this effect is not significant in the resolution of the system. The majority of the reflected ^{13}C beam misses the detector, as the tune for the ^{14}C is 300 V higher than for the reflected ^{13}C beam. However, it may be possible to adjust the positioning of the detector, so that the ^{14}C exits slightly off-axis, to further increase its separation for the interference. This adjustment might be too small to make any significant difference before ^{14}C clips on the exit to the ESA resulting in loss and an additional separation, such as in additional dipole magnet, might be required.

5. Conclusion

The SUERC SSAMS has been successfully rebuilt to accommodate an additional low energy ESA and second ion source injector. The ESA has improved performance by removing the oxygen inference and reducing the source vacuum related background, which in turn allows for a higher productivity of the machine while maintaining reliability in routine measurement. A second interference has been potentially identified as a ^{13}C beam reflected from the plates of the ESA.

Acknowledgements

This work was supported by the NERC Research Council.

References

[1] S.P.H.T. Freeman, A. Dougans, L. McHargue, K.M. Wilcken, S. Xu, Performance of the new single stage accelerator mass spectrometer at the SUERC, Nucl. Instr. Meth. Phys. Res. B 266 (2008) 2225.
[2] K.M. Wilcken, S.P.H.T. Freeman, S. Xu, A. Dougans, Single-stage accelerator mass spectrometer radiocarbon-interference identification and positive-ionisation characterisation, Nucl. Instr. Meth. Phys. Res. B 294 (2013) 353–355.
[3] S.P.H.T. Freeman, G.T. Cook, A. Dougans, P. Naysmith, K.M. Wilcken, S. Xu, Improved SSAMS performance, Nucl. Instr. Meth. Phys. Res. B 268 (2010) 715–717.
[4] K.M. Wilcken, S.P.H.T. Freeman, S. Xu, A. Dougans, Attempted positive ion radiocarbon AMS, Nucl. Instr. Meth. Phys. Res. B 268 (2010) 712–714.
[5] S. Xu, A. Dougans, S.P.H.T. Freeman, C. Maden, R. Loger, A gas ion source for radiocarbon measurement at SUERC, Nucl. Instr. Meth. Phys. Res. B 259 (2007) 76–82.
[6] S.P.H.T. Freeman, R.P. Shanks, Radiocarbon positive-ion mass spectrometry, Nucl. Instr. Meth. Phys. Res. Sect. B 361 (2015) 229–232.
[7] G. Skog, The single stage AMS machine at Lund University: status report, Nucl. Instr. Meth. Phys. Res. B 259 (2007) 1–6.